# Argon density measurements from charge–exchange spectroscopy

D. G. Whyte, R. C. Isler, M. R. Wade, D. R. Schultz, P. S. Krstic, C. C. Hung, and W. P. West

Citation: Physics of Plasmas **5**, 3694 (1998); doi: 10.1063/1.872979
View online: http://dx.doi.org/10.1063/1.872979
View Table of Contents: http://scitation.aip.org/content/aip/journal/pop/5/10?ver=pdfcov
Published by the AIP Publishing



# Argon density measurements from charge–exchange spectroscopy

D. G. Whyte
*University of California at San Diego, San Diego, California 92093*

R. C. Isler, M. R. Wade, D. R. Schultz, and P. S. Krstic
*Oak Ridge National Laboratory, Oak Ridge, Tennessee 37831*

C. C. Hung
*Alabama A&M University, Normal, Alabama 35762*

W. P. West
*General Atomics, San Diego, California 92186-5068*

(Received 28 April 1998; accepted 12 May 1998)

Charge–exchange spectroscopy is widely used to determine the profiles of fully stripped low-*Z* ions (carbon, oxygen, neon) in fusion plasmas. Continuing interest in the use of heavier impurities for radiative cooling in boundaries and divertors of fusion plasmas has encouraged the expansion of this technique for elements such as argon which are not completely burned out in present machines. As a first step, it has been necessary to predict the wavelengths of transitions from Ar XVI to Ar XVIII from theoretical calculations. Several of these have been detected in the DIII-D tokamak [*Plasma Physics Controlled Nuclear Fusion Research*, 1986 (International Atomic Energy Agency, Vienna, 1987), Vol. I, p. 159] subsequent to argon puffing into neutral-beam injected plasmas, and the experimentally determined wavelengths are in good agreement with the predicted values. Argon ion densities have been determined using recent Classical Trajectory Monte Carlo (CTMC) computations of the charge–exchange cross sections, and some radial profiles for specific ionization stages have been measured. © *1998 American Institute of Physics.* [S1070-664X(98)03810-5]

## I. INTRODUCTION

The possibility of dissipating major fractions of the power losses from fusion reactors through radiation, rather than through conduction to divertor target plates, is under investigation in many tokamak laboratories. In addition to using intrinsic impurities, such as carbon, for this purpose, there is also great interest in exploiting rare gases which may prove more effective for cooling. It is crucial, of course, that such deliberately injected impurities be well confined to the divertor region or to a radiating edge mantle so that they neither produce unacceptable levels of emission power losses in the cores of reacting plasmas nor significantly dilute the concentration of hydrogen isotopes. In order to assess the use of argon for this purpose, several recent experiments on the DIII-D tokamak[1] have been performed to measure the compression of this impurity between the core and the divertor pumping plenum and also to assess the efficiency of pumping for inhibiting migration back into the main plasma.[2,3]

These investigations require evaluations of argon concentrations inside the separatrix. At no radius in the plasmas studied, which have central temperatures in the 2–3 keV range, is this element completely ionized, and $Ar^{16+}$, $Ar^{17+}$, and $Ar^{18+}$ are the main constituents over most of the radius. Although the radiating species, $Ar^{16+}$ and $Ar^{17+}$, could be detected from the resonance lines near 4 Å,[4] the fully stripped ions can only be observed through charge–exchange excitation (CXE) from neutral deuterium beams, a technique that has proven very useful for determining the concentrations of low-*Z* elements.[5] Argon densities must be kept relatively low to minimize dilution and to avoid radiative collapse, so CXE emissions are weak compared to those from carbon, the dominant intrinsic impurity. The present studies have explored the feasibility of detecting the three central argon ion species by using modulated neutral-beam injection (NBI) to separate CXE lines from the background. Densities of all three major ion species have been evaluated from soft x-ray transitions by employing Classical Trajectory Monte Carlo (CTMC) calculations of charge transfer cross sections,[6–8] and radial profiles of $Ar^{16+}$ have been determined from visible spectra. The main purposes of this paper are to present the wavelengths of spectral lines useful for CXE studies, to tabulate the relative probabilities of exciting these transitions, and to establish some guidelines for the minimum measurable argon densities in the DIII-D tokamak.

## II. SPECTRAL FEATURES

Charge–exchange spectroscopy in the DIII-D tokamak is performed in both the vacuum ultraviolet (VUV) and visible regions of the spectrum. VUV lines (80 Å–1200 Å) are monitored by a tangentially viewing SPRED (Survey, Poor Resolution, Extended Domain) spectrometer.[9] Its optic axis crosses a neutral particle beam approximately 7 cm outside the magnetic axis of typical plasmas, and the detected signals are localized within a radial span of 3 cm. The visible system (3500 Å–8000 Å), which is used routinely to measure ion temperature and rotation profiles, incorporates an array of sightlines that currently intersect a neutral beam in forty dif-

 

TABLE I. Predicted wavelengths (Å) of $\Delta n=1$ transitions (with statistical *l*-distribution averaging) in Ar XVI–Ar XVIII. Observed lines are denoted by*; lines observed but blended with transitions from other impurities are indicated by #. Measurement wavelengths are denoted in parentheses.

| Transition | Ar XVIII | Ar XVII | Ar XVI |
|---|---|---|---|
| 5–4 | 124.8* (124.98±.04) | 140.0* | 158.1* |
| 6–5 | 229.9* | 257.8* | 291.1# |
| 7–6 | 381.4* | 427.6* | 482.8* |
| 8–7 | 587.7# | 658.9* | 743.9* |
| 9–8 | 857.3* | 961.2 | 1085.1 |
| 10–9 | 1198.6 | 1343.8 | 1517.1 |
| 11–10 | 1620.1 | 1816.4 | 2049.9 |
| 12–11 | 2129.5 | 2387.5 | 2695.3 |
| 13–12 | 2736.49 | 3067.98 | 3463.56* (3463.64±0.1) |
| 14–13 | 3448.92* (3448.8±0.15) | 3866.69 | 4365.23* (4365.53±0.04) |
| 15–14 | 4275.23 | 4793.08 | 5411.03 |
| 16–15 | 5223.87 | 5856.60 | 6611.65 |
| 17–16 | 6303.273 | 7066.73 | 7977.76 |

ferent locations.[10] The integration time for the multichannel charge-coupled devices (CCD's) employed as a detector on these instruments is 5 ms.

The $\Delta n=1$ transitions constitute the strongest CXE lines, and their wavelengths can be predicted with adequate accuracy for the available spectroscopic diagnostics by assuming the wave functions of the highly excited levels of Ar XVI–Ar XVIII are hydrogenic. The simple Rydberg formula is adequate to predict the VUV wavelengths, but a relativistic calculation[11] is required to obtain the visible wavelengths with the necessary precision. Calculated wavelengths (with statistical *l*-mixing) are listed in Table I, and those that have actually been observed are marked with an asterisk.

A VUV spectrum from 80 Å to 240 Å for an argon seeded discharge with 8 MW NBI is shown in Fig. 1(a). (All emission rates are expressed in gigarayleighs where $1\ \mathrm{GR}=10^{15}$ photons/cm$^2$ s.) In this shot, injected argon levels are great enough that the increased radiation is distinctly observable by the bolometer arrays. The Ar XV (beryllium-like) resonance line at 221 Å is by far the brightest feature observed. This line is produced by electron excitation in the plasma periphery. The beam is turned on and turned off alternately in 10 ms intervals, and C VI transitions at 182 Å and 134 Å produced by charge–exchange with $C^{6+}$ are also evident in Fig. 1(a) which was recorded during the beam-on part of the cycle. Because the CCD framing rate is not synchronized to the beam modulation, only one 5 ms data acquisition period out of four corresponds to an interval when the beam is either active or inactive for the whole period. The weaker argon charge–exchange lines are more difficult to distinguish than the carbon lines. By subtracting signals recorded during the beam-off part of the cycle from those obtained during the beam-on interval, the charge–exchange transitions stand out more clearly. Figure 1(b) shows the resulting spectrum integrated over a 0.5 s interval before argon is introduced; only carbon and oxygen transitions are observed. After argon injection [Fig. 1(c)], the additional CXE

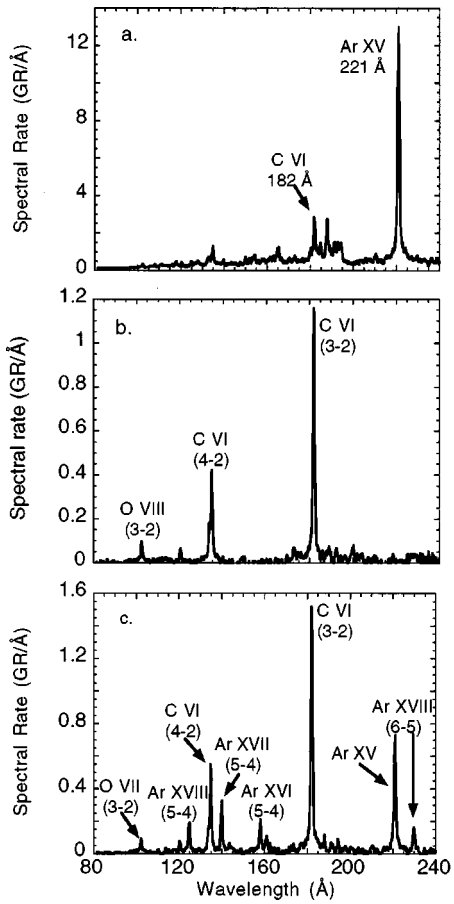


FIG. 1. (a) Raw spectra during a beam-on period after argon injection. The Ar XV line is electron excited; the C VI line is mainly produced by charge exchange. (b) and (c) Average CXE emissions before (0.5 s average) and after (1.0 s average) argon injection. The data are obtained by subtracting signals during beam-off periods from those recorded during beam-on periods.

lines from the $n=5$ to $n=4$ transitions of the three ion species in the center of the plasma are readily discerned at the predicted wavelengths. A residual signal from Ar XV is also evident, although impurity transport modelling indicates very little $Ar^{15+}$ in the plasma center. It appears that this residual must arise from periodic variations in edge conditions as a result of neutral-beam modulation rather than directly from CXE.

Time histories of the $n=5-n=4$ CXE lines smoothed over 20 data points (400 ms) are shown in Fig. 2 together with the evolution of the Ar XV 221 Å transition. Because of the low emission rate, the CXE data are relatively noisy, although bright enough for density measurements. The uncertainty at any given time for the Ar XVII line, which is the brightest of the three, appears to be near 20%.

The VUV lines are useful only for characterizing ion densities near the center of the machine, but radial profiles can be obtained from the visible spectrometer array providing signals are strong enough. Although cross sections for producing the visible transitions are much smaller than those for exciting VUV lines, the greater efficiency of optical components in the visible region can compensate for the differences. A spectrum around the 4365.5 Å line of Ar XVI is

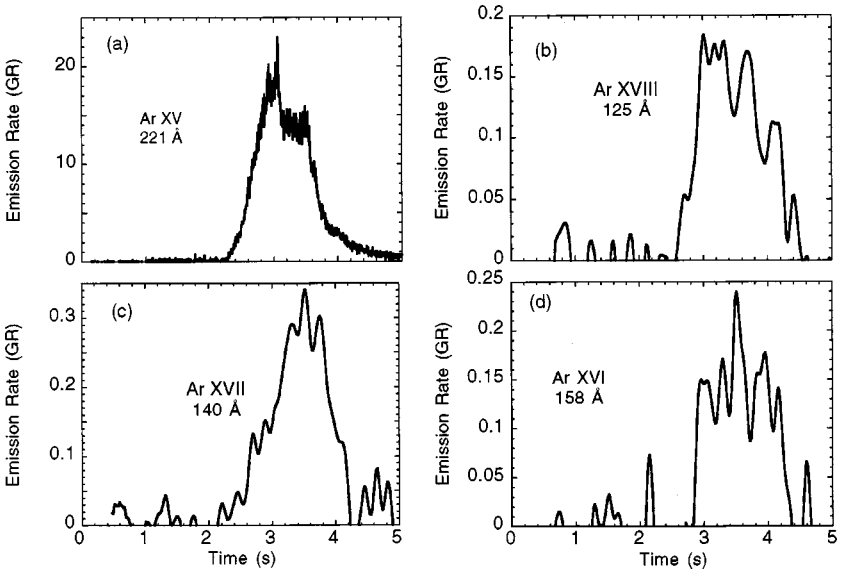


FIG. 2. Temporal evolution of electron excited (Ar XV) and CXE produced (Ar XVIII, Ar XVII, and Ar XVI) spectral lines.

shown in Fig. 3(a) for a discharge with only a trace amount of argon, i.e., increased radiation is observed only weakly on the bolometer arrays. The field of view is not through the plasma center for this case but is tangent at about one-half of the plasma minor radius where the $Ar^{16+}$ is peaked as will be discussed in Sec. III. Despite being near the high-wavelength wing of the strong $D\gamma$ transition, it is observable even without subtraction of the beam-off from the beam-on periods. With this subtraction, Fig. 3(b), the underlying background is eliminated so the line stands out even more clearly. The signal is much weaker near the center of the core plasma where the beam attenuation is more severe and the $Ar^{16+}$ density is significantly less than the peak value. A similar set of uncalibrated visible spectra (with beam-off subtraction) is shown for the region near 3450 Å in Fig. 4. This wavelength region is useful because it contains CXE lines of two argon charge states (Ar XVIII–3448.8 A, Ar XVI–3463.6 Å) and also a line of the dominant intrinsic impurity, carbon (C VI–3433.6 Å). In comparing spectra from the edge and central regions, it is apparent that the $Ar^{+18}$ charge state is relatively more concentrated in the central plasma, as expected (see Sec. III). A strong, unidentified, electron excited line (3453.53 Å) from the plasma periphery makes extraction of the 3448 Å line difficult in these spectra. The broader line shapes also indicate the expected higher ion temperatures in the central plasma.

Accurate wavelengths of the predicted CXE lines are of interest to verify the one-electron atom assumption for the highly excited states; precision is also important for rotation velocity measurements using Doppler shifts of the lines. Ex-

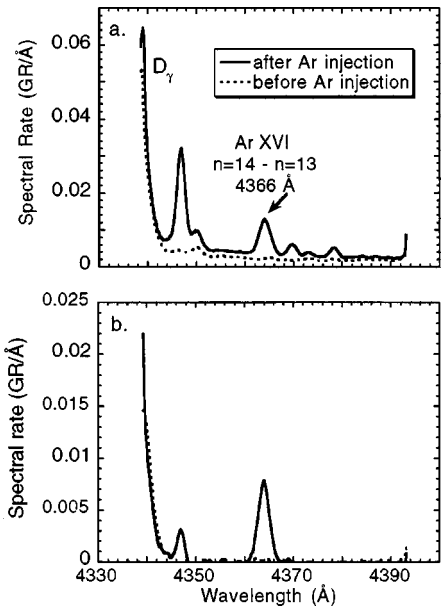


FIG. 3. (a) Raw spectrum around the 4366.9 Å line of Ar XVI. (b) Spectrum obtained by subtracting beam-off data from beam-on data.

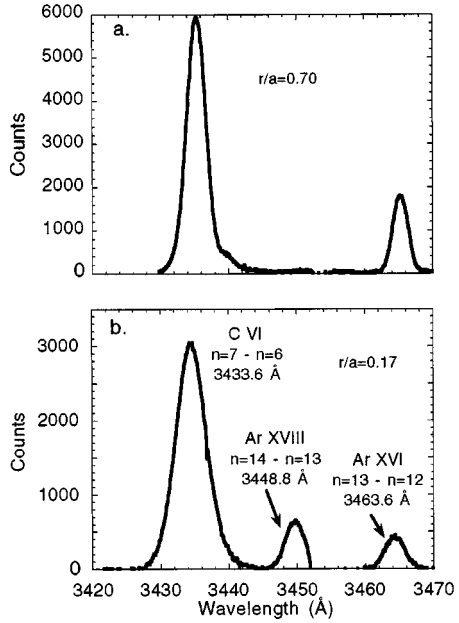


FIG. 4. Uncalibrated CXE spectra (beam-on minus beam-off) from the 3450 Å region showing argon and carbon CXE lines from the center and the edge of a DIII-D plasma.

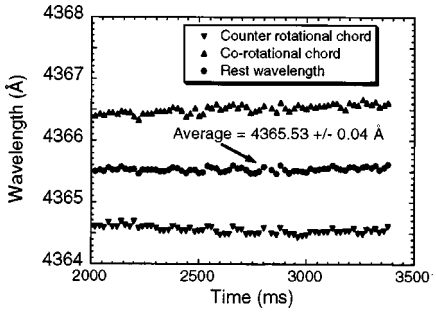


FIG. 5. Experimental measurements of the wavelength of the Ar XVI ($n=14-n=3$) transition from co- and counter-directional viewing chords as a function of time. The rest wavelength is given by the average of the two measurements.

perimentally determined wavelengths are included in Table I for several transitions. They are deduced from measurements along two chords which are oriented in opposite viewing directions but which have the same tangency radius in the plasma. Because of beam-driven plasma rotation the lines are shifted to the red or the blue end of the spectrum by equal increments and the rest wavelength is the average of the two. Neon lamp fiducials are used for the wavelength calibration of the spectrometers. The measured wavelengths and the average are shown as a function of time in Fig. 5. The Doppler shifts from the two chords diverge slightly during the course of the discharge, but the inferred rest wavelength is constant at 4365.53 Å. The rest wavelength of the Ar XVI ($n=13-n=12$) transition was similarly determined to be 3463.64 Å. Other results are less certain due to lack of spectral intensity (for the Ar XVIII, $n=14-n=13$ transition) or data (for the VUV lines) at positions of overlapping counter-directional chords. In this case, results were obtained by assuming that all argon ion species have the same rotation velocity and by correcting the spectra according to the measured central plasma rotation velocity from the Ar XVI 4365.53 Å line. In general, the agreement is satisfactory between the predicted and measured wavelengths, although the two predictions for the three-electron configuration (Ar XVI) are both somewhat higher than the measured values. The Ar XVIII ($n=5-n=4$) measured wavelength is probably dominated by the $5g-4f$ transition (124.95 Å) due to lack of *l*-mixing, although the SPRED instrument lacks sufficient resolution to verify this hypothesis.

## III. CHARGE–EXCHANGE CROSS SECTIONS AND ION CONCENTRATIONS

The CTMC cross sections presented in Table II illustrate the relative probability of populating the various *n*-levels of the product argon ions by charge exchange at a collision energy of 37.5 keV/amu. For this case, levels 8, 9, and 10 are most likely to be directly populated, whereas the $n=5-n=4$ transitions result almost entirely from cascades. Effective emission cross sections for $\Delta n=1$ transitions are shown in Table III. These are computed from *n*, *l*-resolved cross sections[12] under the assumptions of negligible state mixing[5] and no contribution from excited beam particles.[13] Sampson's criterion[14] indicates that full state mixing probably exists for levels higher than 17, 16, and 15, respectively, in Ar XVIII, Ar XVII, and Ar XVI. Partial mixing may begin to appear in levels 10–11[15] but is not expected to alter the emission cross section for the $n=5-n=4$ transitions very much. It should be taken into account, however, when analyzing visible-line data to obtain absolute ion densities. VUV cross sections as a function of energy are presented in Fig. 6, where they are seen to have maxima around 50 keV/amu, an energy just above that of the deuterium beams on DIII-D.

TABLE II. *n*-resolved charge–exchange cross sections ($10^{-15}$ cm$^2$) for an energy of 37.5 keV/amu. Numbers in parentheses are the exponents of 10 by which the listed cross sections must be multiplied.

| *n*-level | Ar XVIII | Ar XVII | Ar XVI |
|---|---|---|---|
| 4 | 3.96 (−5) | 3.01 (−4) | 5.36 (−4) |
| 5 | 3.48 (−3) | 8.67 (−3) | 1.77 (−2) |
| 6 | 6.58 (−2) | 1.25 (−1) | 2.35 (−1) |
| 7 | 5.00 (−1) | 7.77 (−1) | 1.13 |
| 8 | 1.67 | 2.11 | 2.44 |
| 9 | 2.85 | 2.74 | 2.30 |
| 10 | 2.18 | 1.47 | 9.10 (−1) |
| 11 | 7.98 (−1) | 5.26 (−1) | 3.44 (−1) |
| 12 | 3.25 (−1) | 2.19 (−1) | 1.52 (−1) |
| 13 | 1.53 (−1) | 1.11 (−1) | 7.96 (−2) |
| 14 | 8.21 (−2) | 5.97 (−2) | 4.60 (−2) |
| 15 | 4.79 (−2) | 3.60 (−2) | 2.95 (−2) |
| 16 | 3.09 (−2) | 2.56 (−2) | 1.90 (−2) |
| 17 | 1.98 (−2) | 1.62 (−2) | 1.35 (−2) |

Ion densities are derived from measured signals and emission cross sections after calculating the fractions of the original beam currents which reach the spectrometer field of view. In addition to the influence of the working gas particles on the beam attenuation, the stopping powers of carbon and argon themselves are taken into account by using theoretical impurity profiles predicted from the STRAHL transport code[16] and iterating the calculation until it reaches an asymptotic solution. In the experiment analyzed here, the total argon density on the magnetic axis at 3.5 s is found to be $0.18\times10^{12}$/cm$^3$, and the carbon density is $0.15\times10^{13}$/cm$^3$. Pro-

TABLE III. Emission cross sections ($10^{-15}$ cm$^2$) for an energy of 37.5 keV/amu.

| Transition | Ar XVIII | Ar XVII | Ar XVI |
|---|---|---|---|
| 2–1 | 7.60 | 7.12 | 6.64 |
| 3–2 | 6.21 | 5.77 | 5.34 |
| 4–3 | 5.41 | 5.01 | 4.60 |
| 5–4 | 4.71 | 4.34 | 3.98 |
| 6–5 | 4.11 | 3.79 | 3.48 |
| 7–6 | 3.66 | 3.41 | 3.18 |
| 8–7 | 3.40 | 3.20 | 2.95 |
| 9–8 | 3.09 | 2.67 | 2.12 |
| 10–9 | 2.05 | 1.42 | 0.891 |
| 11–10 | 0.810 | 0.484 | 0.275 |
| 12–11 | 0.256 | 0.145 | 0.0814 |
| 13–12 | 0.0810 | 0.0479 | 0.0286 |
| 14–13 | 0.0282 | 0.0182 | 0.0119 |
| 15–14 | 0.0605 | 0.004 61 | 0.003 77 |
| 16–15 | 0.0380 | 0.003 15 | 0.002 39 |
| 17–16 | 0.0240 | 0.001 98 | 0.001 66 |

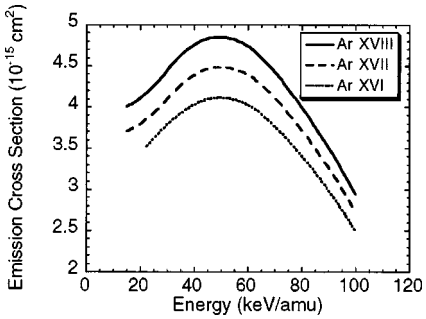


FIG. 6. Emission cross sections for the $n=5-n=4$ transitions of the three highest argon ion stages as a function of collision energy.

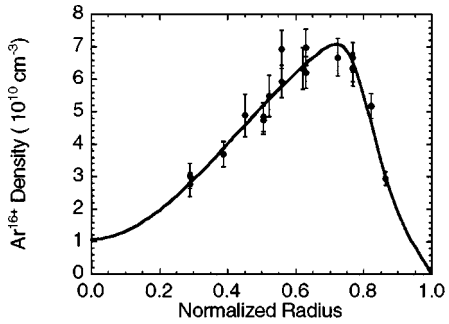


FIG. 8. Measured profile of $Ar^{16+}$ (solid circles). The curve is the best fit through the measured points.

portionalities among the three argon ions, $Ar^{18+}$:$Ar^{17+}$:$Ar^{16+}$, are 0.49:1.00:0.62. These results indicate contributions of 0.65 and 0.60, respectively, for argon and carbon to $Z_{\text{eff}}$ at the magnetic axis where the electron density is $7.5\times10^{13}/\text{cm}^3$. The transport parameters employed in STRAHL are a diffusion coefficient $D=5000\ \text{cm}^2/\text{s}$ and an inward convection velocity $V_c=-0.6Dr/a^2$, where $r$ and $a$ are the radial coordinate and the minor radius for a circular plasma having the midplane dimensions of the DIII-D plasma. With these parameters, the total impurity density profiles are well matched to the electron density profile as typically observed in H-mode plasmas with ELMs (Edge Localized Modes) such as those used for the present studies. Also, some uncertainty in the radial impurity distributions does not lead to serious errors in deducing the central densities at low concentrations since the beam attenuation depends mainly on the working gas particles. The normalized concentrations predicted by the transport code as a function of radius are shown in Fig. 7. They are in the proportions 0.64:1.00:0.62 at the plasma center and compare well to experimental results.

The profile of $Ar^{16+}$ as determined from the 4365.5 Å transition is shown in Fig. 8. Its variation as a function of radius qualitatively resembles the prediction of the transport code as plotted in Fig. 7 for the discharge with the strong argon injection. Although absolute densities are plotted, they have been calculated without any of the corrections that may be needed for the visible lines. Evaluating the contributions from beam particles in excited states, partial state mixing within a given $n$-level of the radiating ions, reexcitation of high energy levels by electron collisions in dense plasmas, and plume effects constitute problems beyond the scope of the present analysis.

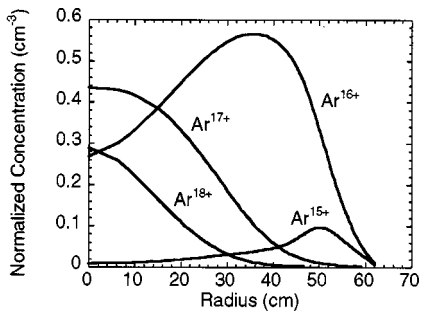


FIG. 7. Relative argon ion profiles calculated from the STRAHL code. The total argon density is normalized to unity at $r=0$.

## IV. SUMMARY

$Ar^{18+}$, $Ar^{17+}$, and $Ar^{16+}$ have been detected through VUV and visible CXE lines in the center of DIII-D discharges by using modulated neutral beams. Argon ion densities are extracted with the aid of theoretical CTMC charge–exchange cross sections, and their ratios agree with the ratios predicted by the STRAHL impurity transport code. Maximum total argon densities measured subsequent to gas puffing of the impurity are 0.24% of the central electron density, $7.5\times10^{13}/\text{cm}^3$. The uncertainty is estimated to be 20%. It appears possible to measure to about the 0.1% level at this density with an uncertainty of 50%. In lower density plasmas where the beam attenuation is not so severe, the sensitivity should be less limited. The Ar XVI line at 4366.9 Å is well isolated from other visible transitions and has proven useful for measuring radial profiles.

## ACKNOWLEDGMENTS

This work was performed for the U.S. Department of Energy under Contract No. DE-AC05-96OR22464 with Oak Ridge National Laboratory, managed by Lockheed Martin Energy Research Corp. and DE-AC03-89ER51114 with General Atomics.

[1] J. Luxon, P. Anderson, F. Batty *et al.*, *Plasma Physics Controlled Nuclear Fusion Research*, Proceedings of the 11th International Conference, Tokyo, 1986 (International Atomic Energy Agency, Vienna, 1987), Vol. I, p. 159.
[2] M. R. Wade, J. T. Hogan, S. L. Allen, N. H. Brooks, D. N. Hill, R. Maingi, M. J. Schaffer, J. G. Watkins, D. G. Whyte, R. D. Wood, and W. P. West, ''Impurity Enrichment Studies with Induced Scrape-Layer Flow on DIII-D,'' General Atomics Report GA-A22698, March 1998.
[3] M. J. Schaffer, M. R. Wade, R. Maingi, P. Moniet-Garbet, W. P. West, D. G. Whyte, R. D. Wood, and M. A. Mahdavi, J. Nucl. Mater. **241–243**, 585 (1997).
[4] R. T. Snider, N. H. Brooks, and N. Bogatu, Bull. Am. Phys. Soc. **42**, 1977 (1997).
[5] R. C. Isler, Plasma Phys. Controlled Fusion **36**, 171 (1994).
[6] R. E. Olson, Phys. Rev. A **24**, 1726 (1981).
[7] R. E. Olson and D. R. Schultz, Phys. Scr. **T28**, 71 (1989).
[8] D. R. Schultz and P. S. Krstic, ''Atomic and Plasma-Material Interaction Data for Fusion'' (Supplement to the Journal Nuclear Fusion), Vol. 6, 173 (1996).
[9] R. J. Fonck, A. T. Ramsey, and R. V. Yelle, Appl. Opt. **21**, 2115 (1982).

[10]P. Gohil, K. H. Burrell, R. J. Groebner, J. Kim, W. C. Martin, E. L. McKee, and R. P. Seraydarian, in *Proceedings of the 14th IEEE/NPSS Symposium on Fusion Engineering*, California, 1991 (Institute of Electrical and Electronics Engineers, New Jersey, 1992), Vol. II, p. 1199.
[11]J. D. Garcia and J. E. Mack, J. Opt. Soc. Am. A **55**, 654 (1965).
[12]CTMC results for *n*- and *n*, *l*-resolved state selective charge transfer cross sections have been tabulated for atomic hydrogen colliding with $Ar^{15+}$, $Ar^{16+}$, $Ar^{17+}$, and $Ar^{18+}$ at energies of 15, 22.5, 37.5, 45, 60, 80, and 100 keV/amu. They are available from the Controlled Fusion Atomic Data Center, Physics Division, Oak Ridge National Laboratory, Box 2008, Oak Ridge, TN 37831.
[13]R. C. Isler and R. E. Olson, Phys. Rev. A **37**, 3399 (1988).
[14]D. H. Sampson, J. Phys. B **10**, 749 (1977).
[15]R. J. Fonck, D. S. Darrow, and K. P. Jaehing, Phys. Rev. A **29**, 3288 (1984).
[16]K. Lackner, K. Behringer, W. Engelhardt, and W. Wunderlich, Z. Naturforsch. **37a**, 931 (1982).